Journal of Functional Materials and Applied Engineering

Research Paper

Construction and Performance of Conductive Triple-Network Hydrogel Dressing

Alexander Popov[1], Maria Garcia[1,*], Elif Yilmaz[2], James Wilson[2]

[1] Institute for w=Environmental Engineering, University of Cambridge, United Kingdom
[2] University of Wollongong, Wollongong, Australia
*Corresponding author: AP32@cam.ac.uk; Mg-B@cam.ac.uk; Yilmaz@gmail.com; Wilson@gmail.com

Abstract. Chronic wounds present significant clinical challenges due to factors such as microbial infection and an imbalanced healing microenvironment, making the healing process difficult and necessitating the development of novel dressings capable of providing both dynamic biological therapy and electrical signal modulation. However, existing hydrogel materials still face considerable difficulties in integrating multiple functionalities, including bioactivity, mechanical flexibility, conductivity, and stimuli-responsive release. To address this, this study proposes a multi-network synergistic design strategy. By combining carboxymethyl agarose (CMA), sodium alginate (SA), and polyvinyl alcohol (PVA), and incorporating multivalent ions Ca2+, Mg2+, and Zn2+, a triple-network hydrogel (CaPSC-MZ) with ion-conductive and pH-responsive ion-release capabilities has been successfully constructed. The results demonstrate that through the modification of agarose and the multi-network structural design, the CaPSC-MZ hydrogel exhibits an average pore size of approximately 91.47 μm, providing favorable swelling properties (50.07%) and a high water retention capacity (13.13%). The CaPSC-MZ hydrogel also demonstrates excellent foldability. Moreover, the release of Ca2+, Mg2+, and Zn2+is enhanced under acidic conditions, achieving a conductivity of up to 24.81 mS/cm. Additionally, CCK-8 experiments confirm that the CaPSC-MZ hydrogel exhibits excellent biocompatibility and promotes cell proliferation. Therefore, this study provides a new material design strategy for developing smart wound dressings with integrated electrical conduction, dynamic therapeutic functionality, and mechanically adaptive properties, showing promising potential in the field of wound management.

Keywords: *wound dressing; multifunctional hydrogel; foldable; conductive hydrogel; triple-network dressing*

Received on 02 June 2025, Accepted on 02 August 2025, Published on 15 September 2025

1 Introduction

Skin injury and its associated health risks constitute one of the critical factors affecting human health, imposing a substantial burden on global healthcare systems. Particularly, chronic wounds caused by bacterial infections have emerged as a major clinical challenge[2]. The wound healing process typically encompasses four sequential yet overlapping stages: hemostasis, inflammation, proliferation, and remodeling[3]. Notably, intact skin provides external protection to tissues; once compromised, the risk of colonization by environmental pathogenic microorganisms (e.g., bacteria and viruses) increases dramatically, triggering persistent inflammatory responses, inhibiting cell proliferation, and delaying the healing process. Therefore, providing a suitable environment for wounds plays a pivotal role in promoting tissue repair and wound healing[4].

Hydrogels, characterized by a three-dimensional network structure resembling the extracellular matrix, excellent water content, and good biocompatibility, are widely regarded as ideal candidate materials for wound dressings. Agarose is a polysaccharide extracted from algae, renowned for its exceptional biocompatibility. Huang et al.[5]synthesized carboxymethyl agarose (CMA) via carboxymethylation of agarose; the introduced carboxyl groups not only enhanced the material's functionality but also provided abundant sites for loading

bioactive components. However, CMA forms hydrogels reliant on hydrogen bonding, exhibiting low mechanical strength and a gelation process highly sensitive to temperature, rendering it difficult to adapt to the complex and variable wound environment. Polyvinyl alcohol (PVA) possesses good water absorbency, flexibility, and mechanical strength, and is widely utilized in drug delivery, biosensors, and wound dressings. For instance, Huang et al.[7]reported a PVA-chitosan double-network hydrogel, wherein the PVA network contributed excellent stretchability and tissue adhesion, effectively preventing postoperative abdominal wall adhesions. Therefore, combining PVA with CMA is expected to significantly improve the mechanical properties of CMA while retaining its functionality.

In recent years, the role of bioelectrical signals in tissue repair has garnered increasing attention. Cellular activities inherently depend on endogenous electrical signal transduction; applying external electrical stimulation to wounds can mimic and augment this process, thereby promoting cell proliferation and migration[8]. To impart conductivity to hydrogels, researchers typically incorporate conductive fillers[9]. For example, Hou et al.[10]embedded silver nanowires into methacrylated gelatin (GelMA/AgNWs) to develop a novel conductive hydrogel wound dressing for accelerated skin wound healing. Li Liang et al.[11]enhanced conductivity via carbon nanotubes to construct a self-healing PVA-based conductive hydrogel, achieving a maximum conductivity of 2.56 S/m. Although incorporating conductive fillers such as silver nanowires and carbon nanotubes can elevate conductivity, the introduction of these rigid materials often compromises the flexibility of the hydrogel. On the other hand, some studies employ conductive polymers like PEDOT:PSS or liquid metals[12]. For instance, Wang Ming et al.[13]fabricated a PEDOT:PSS-based conductive hydrogel for in vitroelectrocardiogram (ECG) monitoring electrodes. Lin Xingyue et al.[14]compounded liquid metal (LM) with β-cyclodextrin (CD) to initiate the copolymerization of acrylamide (AAm) monomers, thereby enhancing gel conductivity. However, these materials often exhibit weaker biocompatibility, failing to meet the high safety requirements for long-term contact with living tissues such as wounds. To balance conductivity and biocompatibility, Lei et al.[15]incorporated tannic acid (TA) and human-like collagen (HLC) into a PVA hydrogel, utilizing borax for ionic conduction, achieving both conductivity and good biocompatibility. Guan et al.[16]prepared a conductive hydrogel using polydopamine-modified silver nanoparticles, cellulose nanocrystals (CNC), polypyrrole (PPy), and PVA for diabetic wound repair. Nevertheless, these systems are predominantly based on single-network structures, suffering from insufficient drug-loading sites and singular functionality, making stimuli-responsive release challenging. Gong et al.[17]constructed a double-network hydrogel based on poly(2-acrylamido-2-methylpropanesulfonic acid) (PAMPS) and polyacrylamide (PAAm), significantly improving mechanical properties through complementary advantages, providing important insights for constructing multifunctional hydrogels via network structural design. Currently, reports on multi-network hydrogels capable of simultaneously integrating excellent biofunctionality, high flexibility, good conductivity, and biosafety remain scarce; thus, developing such materials holds significant importance.

Sodium alginate (SA), derived from brown algae, is a natural polysaccharide with good biocompatibility. Its molecular chains are rich in carboxyl groups, conferring electronegativity, and can form a stable "egg-box" structure via crosslinking with divalent ions (e.g., Ca2+), endowing the hydrogel with a degree of ionic conductivity. Furthermore, SA exhibits pro-angiogenic potential by releasing pro-angiogenic factors and maintaining the viability of dental pulp stem cells (DPSCs), thereby promoting wound repair. On the other hand, metal ions, as crucial biological signaling molecules, play diverse regulatory roles in the wound healing process[18]. For instance, Ca2+and Li+are essential catalytic or structural elements for certain transcription factors, enzymes, and proteins. Ag+, owing to its excellent antimicrobial properties, is widely used for treating infected wounds. Among them, Mg2+and Zn2+, serving as vital coenzymes, play significant roles in wound healing, including promoting epithelial regeneration, regulating cellular immunity, and facilitating the migration and adhesion of fibroblasts (HSFs). Therefore, introducing bioactive metal ions into the hydrogel system can not only enhance its conductivity but also impart pro-healing functionality.

Based on the aforementioned context, this work designed and fabricated a conductive triple-network hydrogel (CaPSC-MZ) loaded with Ca2+, Mg2+, and Zn2+. This system comprises a triple interpenetrating network constructed from CMA, PVA, and SA. Among these, CMA serves as the functional network, loading Mg2+and Zn2+with pH-responsive release characteristics via its carboxyl groups. SA crosslinks with Ca2+to form a stable ionic network, providing fundamental conductivity. Additionally, benefiting from PVA's contribution, physical crosslinking within PVA confers excellent flexibility and mechanical support to the hydrogel, enabling it to be

folded and stretched to accommodate dynamic skin changes. Through multi-network design and active ion loading, this work establishes a composite hydrogel integrating flexibility, conductivity, pH-responsive release, and pro-healing functions, laying a solid foundation for developing novel smart wound dressings.

2 Experimental Materials and Methods

2.1 Experimental Materials

Ethanol (AR, 99.9%) was purchased from Sinopharm Chemical Reagent Co., Ltd. (Shanghai, China). Agarose (biomolecular grade), isopropanol (AR, ≥99.7%), chloroacetic acid (≥99%), anhydrous calcium sulfate (CaSO4, AR, ≥99.7%), polyvinyl alcohol (PVA, Type 1799, degree of alcoholysis: 98%–99% (molar fraction)), anhydrous magnesium chloride (MgCl2, ≥99.99%), zinc chloride (ZnCl2, ≥98%), and Cell Counting Kit-8 (CCK-8) (MoligandTM) were procured from Aladdin Biochemical Technology Co., Ltd. (Shanghai, China). Sodium alginate (SA, ≥98%) was obtained from Tianjin Yongda Chemical Reagent Co., Ltd. Deionized water was used throughout the experiments.

2.2 Preparation of CMA

Firstly, agarose was modified in this study to introduce carboxyl groups. Since agarose is insoluble in organic solvents, isopropanol was used to disperse it uniformly, forming a suspension to facilitate subsequent reactions. NaOH reacted with hydroxyl groups on agarose to generate alkoxide ions (-ONa) with stronger nucleophilicity. Simultaneously, under alkaline conditions, chloroacetic acid transformed into sodium chloroacetate, which subsequently underwent a nucleophilic substitution reaction with -ONa on agarose, thereby introducing carboxymethyl (-CH2COONa) groups. The chemical reactions are shown in Eqs. (1) and (2):

$$\text{agarose—OH} + \text{NaOH} \rightarrow \text{agarose—O}^{-}\text{Na}^{+} + \text{H}_2\text{O} \quad (1)$$

$$\text{agarose—O}^{-}\text{Na}^{+} + \text{ClCH}_2\text{COONa} \rightarrow \text{agarose—O—CH}_2\text{COONa} + \text{NaCl} \quad (2)$$

The detailed experimental procedure was as follows: 10 g of agarose was magnetically stirred with 100 mL of isopropanol at 24 °C for 30 min. Subsequently, 10.64 g of sodium hydroxide was added to the mixture and stirred continuously at 24 °C for another 30 min. After standing for 5 min, 5 mL of the aforementioned mixture (supernatant) was taken to dissolve 5 g of chloroacetic acid. This dissolved chloroacetic acid solution was then added dropwise to the agarose mixture. After completion of the dropwise addition, magnetic stirring continued for 30 min, followed by stirring at 70 °C for 2 h. Upon reaction completion, the mixture turned brown. After standing for 10 min, CMA solid particles precipitated at the bottom of the beaker. The solid particles were collected, washed 2–3 times with ethanol, freeze-dried, and stored at 4 °C.

2.3 Preparation of CaPSC Hydrogel

Initially, a 2 wt% CMA aqueous solution was prepared by dissolving 4 g of CMA solid particles in 20 mL of deionized water at 70 °C. Subsequently, a 5 wt% SA aqueous solution was prepared in a 65 °C water bath. The PVA solution (10 wt%) was prepared in an oil bath at 90 °C. A CaSO4suspension was prepared (3 g of CaSO4in 20 mL of deionized water). The mixed solution of MgCl2and ZnCl2was formulated as follows: 13.14 g of MgCl2, 14.12 g of ZnCl2, and 20 mL of deionized water. The formulation for CaPSC-MZxwas: 15 mL of PVA solution, 5 mL of SA solution, 10 mL of CMA solution, 0.2 mL of CaSO4suspension, and xmL of the MgCl2/ZnCl2mixed solution. The formulation for CaxPSC-MZ was: 15 mL of PVA solution, 5 mL of SA solution, 10 mL of CMA solution, xmL of CaSO4suspension, and 0.2 mL of the MgCl2/ZnCl2mixed solution. The formulation for CaP2SC-MZxwas: 20 mL of PVA solution, 5 mL of SA solution, 5 mL of CMA solution, 0.2 mL of CaSO4suspension, and xmL of the MgCl2/ZnCl2mixed solution. The formulation for CaxP2SC-MZ was: 20 mL of PVA solution, 5 mL of SA solution, 5 mL of CMA solution, xmL of CaSO4suspension, and 0.2 mL of the MgCl2/ZnCl2mixed solution. Here, x= 0, 0.05, 0.1, 0.15, 0.2, 0.4, 0.6, 0.8.

Taking the preparation of CaPSC-MZ hydrogel as an example, the specific steps were as follows: Firstly, 15 mL of PVA solution, 5 mL of SA solution, and 10 mL of CMA solution were stirred at 70 °C for 30 min to achieve homogeneous mixing of the three networks. Subsequently, 0.2 mL of CaSO4suspension and 0.2 mL of the MgCl2/ZnCl2mixed solution were added to the aforementioned mixture and stirred at 70 °C for another 30 min to ensure uniform distribution of the CaSO4suspension and the MgCl2/ZnCl2mixed solution within the gel matrix. After stirring, the mixture was allowed to stand at room temperature for 2 h to form a preliminary solid gel. This was followed by freezing at −20 °C for 4 h and thawing at room temperature (24 °C) for 1 h, repeating this freeze-thaw cycle three times.

2.4 Structural and Performance Characterization

Fourier transform infrared spectroscopy (FT-IR-850) was employed to characterize agarose and CMA. Agarose and CMA were thoroughly dried, ground, and passed through a 200-mesh sieve. They were then ground together with thoroughly dried potassium bromide (spectroscopic grade) and pressed into pellets for measurement within the wavenumber range of 400–4000 cm−1.

Scanning electron microscopy (SU8010) was utilized to characterize the microstructures of CMA, PVA, CaPSC, and CaPSC-MZ hydrogels. Hydrogel samples were cryo-fractured using liquid nitrogen and then freeze-dried. CMA and PVA samples, due to their poor conductivity, required two rounds of gold sputtering, while CaPSC and CaPSC-MZ hydrogels required one round of gold sputtering.

The swelling properties of the hydrogels were tested to evaluate their capacity to absorb wound exudate. The initial mass (m0) of each hydrogel group was recorded. Subsequently, the hydrogels were immersed in sufficient deionized water, and the mass (md) of the hydrogels was recorded at regular intervals (the surface moisture of the hydrogels was carefully wiped off before each weighing). Each sample was measured in triplicate. The swelling ratio (SR) was calculated using Eq. (3):

$$S_R = \frac{m_d - m_0}{m_0} \times 100\% \qquad (3)$$

The water loss properties of the hydrogels were tested to evaluate their moisturizing capacity for wounds. The initial mass (m0) of each hydrogel group was recorded. Subsequently, the hydrogels were placed in a 24 °C environment, and the mass (mt) was recorded at regular intervals. Each sample was measured in triplicate. The water retention ratio (WR) was calculated using Eq. (4):

$$W_R = \frac{m_t}{m_0} \times 100\% \qquad (4)$$

The release kinetics of Ca2+, Mg2+, and Zn2+were determined using the solvent method. CaPSC-MZ hydrogel samples (4 mL) were immersed in 20 mL of deionized water at different pH values and temperatures. Aliquots were periodically collected and analyzed using inductively coupled plasma optical emission spectrometry (ICP-OES) to determine the ion release amounts at different time points.

The electrical conductivities of hydrogels from different groups were measured using an electrochemical workstation (CHI760F). The hydrogel samples were sandwiched between two platinum plates, with a frequency range of 0.1 Hz to 1 MHz. Impedance data were fitted using ZView 4 software to obtain the solution resistance (RS). The conductivity (σ) was calculated using the formula σ = t/(RSA), where tis the thickness of the hydrogel and Ais the electrode area.

CCK-8 assays were conducted to evaluate the biocompatibility of the hydrogels. Each hydrogel group was immersed in complete culture medium at a ratio of 0.1 g/mL for 24 h. The extract was filtered and used for cell culture. Human skin fibroblasts (HSFs) were seeded into 96-well plates at a density of 1×103cells per well. At predetermined time points (Days 1, 3, 5, and 7 post-treatment), the culture supernatant was collected, and the absorbance (OD value) at 450 nm was measured using a microplate reader.

3 Results and Analysis

3.1 Preparation and Characterization of CMA

Figure 1 presents the Fourier transform infrared spectra of CMA and agarose. Agarose exhibits low-intensity absorption peaks at 910 cm−1and 830 cm−1, attributed to the bending vibrations of C–H in the 3,6-anhydro-α-L-galactopyranosyl residue and the β-D-galactopyranosyl residue, respectively[19]. CMA retains the characteristic O–H peak of agarose at 3449 cm−1. The signal near 2890 cm−1corresponds to the symmetric and antisymmetric stretching vibrations of the polysaccharide backbone[20]. Furthermore, the peaks appearing at 1610 cm−1and 1420 cm−1correspond to the asymmetric and symmetric stretching vibrations of carboxylate groups, respectively, indicating the successful introduction of carboxyl groups. Compared to agarose, the absorption peak intensity of the methylene group in CMA at 1234 cm−1is significantly enhanced, and the low-intensity signal near 1149 cm−1can be attributed to C–O and C–O–H stretching[21]. The aforementioned spectral features collectively demonstrate that CMA successfully introduces –CH2COO– groups while maintaining the integrity of the agarose polysaccharide backbone, thereby enhancing its chemical structural complexity.

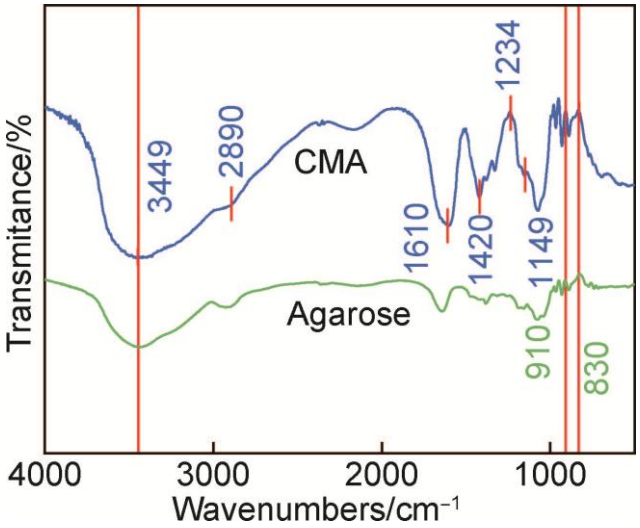

Figure 1 FT-IR spectra of agarose and CMA.

3.2 Preparation and Structure of CaPSC Hydrogel

The CaPSC hydrogel was synthesized via a facile one-pot method. CMA, PVA, and SA were dissolved in deionized water to obtain 2 wt%, 10 wt%, and 5 wt% solutions, respectively, followed by the addition of varying proportions of Ca2+, Mg2+, and Zn2+mixed solutions. Subsequently, the homogeneously mixed solution was poured into silicone molds. After standing for 2 h, three freeze-thaw cycles were performed to yield CaPSC-MZ hydrogels with different formulations.

Figure 2 illustrates the construction mechanism and structural schematic of the CaPSC-MZ triple-network hydrogel. The CaPSC hydrogel comprises three interpenetrating networks. The first network is the CMA network, primarily contributing abundant functional groups to the hydrogel. The CMA molecular chains contain numerous hydroxyl and carboxyl groups, forming a physical crosslinking network via hydrogen bonding and ionic interactions. The second network is the PVA network, functioning to enhance the flexibility and mechanical properties of the hydrogel. PVA molecular chains are also rich in hydroxyl groups. During freezing at −20 °C, water crystallizes, expelling PVA chains into amorphous regions, prompting close proximity of molecular chains and the formation of physical crosslinking points via hydrogen bonds. After multiple freeze-thaw cycles, stable three-dimensional networks form through dense hydrogen-bonded microcrystalline regions between PVA chains. The third network is the SA network, responsible for providing ionic conductivity. SA consists of β-D-mannuronic acid and α-L-guluronic acid units. When guluronic acid units appear consecutively (G-block segments), the spatial arrangement of their carboxyl and hydroxyl groups forms negatively charged cavities

known as the "egg-box" structure. Divalent metal ions (e.g., Ca2+, Mg2+, Zn2+) can embed into these "egg-boxes," crosslinking SA molecular chains via coordination interactions to form an ionic three-dimensional network. Among these, Ca2+exhibits high affinity for G-blocks, rapidly forming coordination crosslinks dominated by ionic bonds. Although the crosslinking mechanisms of the three networks differ, the molecular chains of CMA, PVA, and SA are all rich in hydroxyl groups, enabling them to synergistically form a structurally homogeneous and stable triple-network hydrogel, CaPSC-MZ, through hydrogen bonding and molecular chain entanglement.

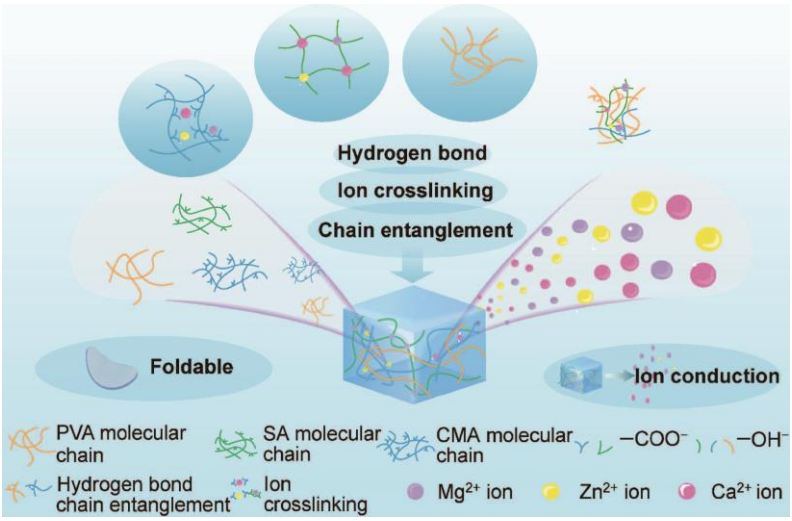

Figure 2 Schematic diagram of the formation mechanism and structure of CaPSC-MZ hydrogel.

Figure 3 presents the SEM images and corresponding pore size distributions of different hydrogels. The CMA single-network hydrogel exhibits a typical porous structure with sparse pores, a pore size distribution ranging from 166.66 to 257.03 µm, and an average pore size of 209.46 µm. In contrast, the PVA single-network hydrogel surface appears relatively smooth, displaying only a few collapsed micropores with a narrow pore size distribution (40.21–48.73 µm) and an average pore size of 44.77 µm. The successfully prepared triple-network hydrogel, CaPSC, influenced by the CMA structure, retains porous characteristics with a pore size distribution of 114.07–146.72 µm and an average pore size of 129.34 µm. Upon further introduction of Mg2+and Zn2+, the pore size of the resulting CaPSC-MZ hydrogel decreases slightly, ranging from 85.18 to 103.96 µm with an average pore size of 91.47 µm. This change can be attributed to the enhanced ionic crosslinking within the network induced by the addition of metal ions, leading to contraction of the polymer chain spacing and a denser structure.

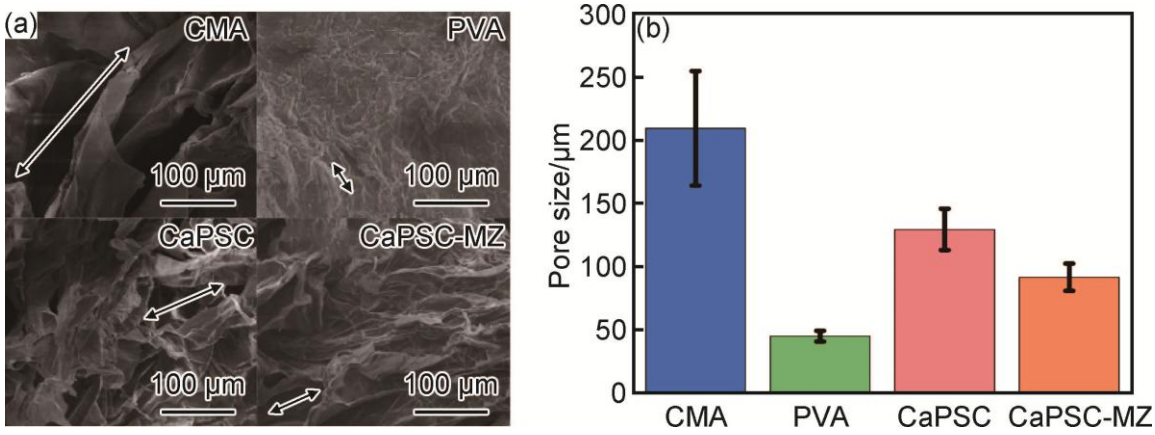

Figure 3 SEM images of CMA, PVA, CaPSC, and CaPSC-MZ hydrogels (a) and their pore sizes (b).

Literature reports indicate that the loose porous structure within hydrogels facilitates cell migration and proliferation, thereby promoting wound healing[22–23]. These sponge-like porous structures can rapidly absorb tissue fluids from wounds, reduce bacterial proliferation, and lower the risk of wound infection. The CaPSC-MZ hydrogel possesses a loose and porous three-dimensional network structure with good air permeability, making it suitable as a wound dressing to provide an appropriate healing environment for wound sites, further accelerating the healing process.

3.3 Water Absorbency and Retention of CaPSC-MZ Hydrogel

Maintaining an appropriate moist environment during wound healing benefits cell migration and repair[24–25]. However, excessive exudate can enlarge the wound area, delay healing, and increase pain and infection risks. Therefore, a key factor in evaluating hydrogels as wound dressings lies in balancing water retention and absorbency.

Figure 4(a) illustrates the change in water retention performance of CaPSC and CaPSC-MZ hydrogels over time at 24 °C. As time progressed, the water retention rates of both sample groups gradually declined. However, the introduction of Mg2+and Zn2+significantly improved the water retention capacity of CaPSC-MZ. This is attributed to the enhanced crosslinking density induced by metal ions, which suppresses water evaporation and helps maintain a higher water retention rate. This result aligns with the observation from SEM that CaPSC-MZ possesses a denser pore structure compared to CaPSC.

To further investigate the influence of network structure on water retention, this study compared the water retention rates of PVA, CMA, CaPSC, and CaPSC-MZ at the 24-hour mark (Figure 4(b)). The PVA single-network hydrogel, owing to its dense pore structure (average 44.77 μm), exhibited the highest water retention, with an average rate of 20.99%. Conversely, the CMA single-network hydrogel, characterized by the largest pore size, showed the lowest water retention rate after 24 hours, merely 1.08%. In comparison, the water retention rates of CaPSC and CaPSC-MZ were 7.74% and 13.13%, respectively, demonstrating the positive contribution of the triple-network structure and its metal ion crosslinking to moisture preservation.

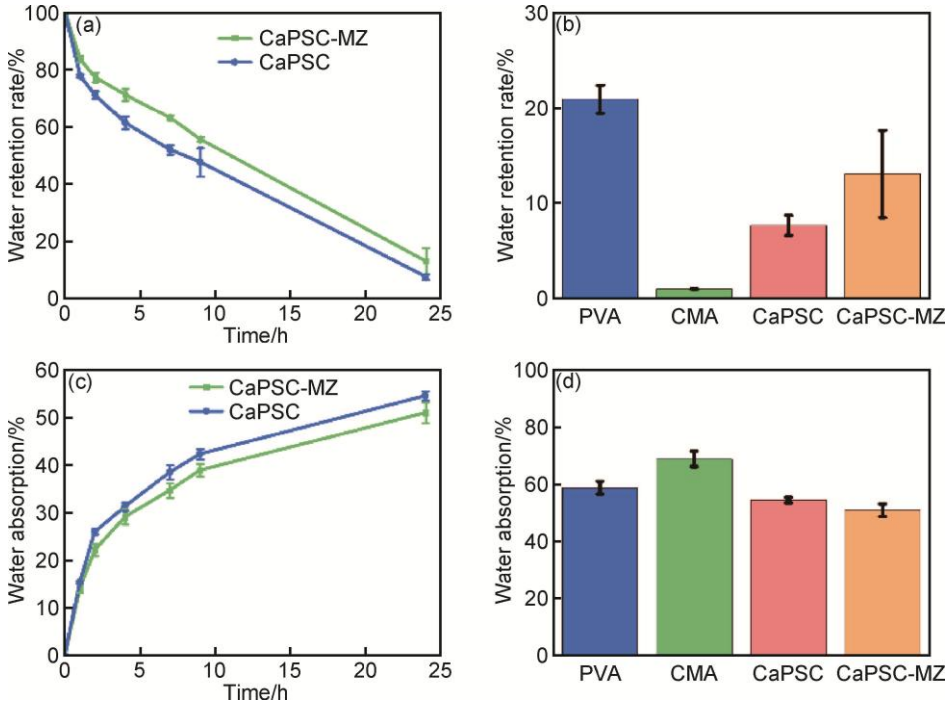

Figure 4 Water retention of CaPSC and CaPSC-MZ (a), water retention equilibrium of CMA, PVA, CaPSC, and CaPSC-MZ (b), swelling of CaPSC and CaPSC-MZ (c), swelling equilibrium of CMA, PVA, CaPSC, and CaPSC-MZ (d).

Enhanced water retention typically accompanies a corresponding reduction in water absorbency. As shown in Figure 4(c), the swelling ratios of both CaPSC and CaPSC-MZ gradually increased with prolonged immersion time. Although the swelling ratio of CaPSC was slightly higher than that of CaPSC-MZ, CaPSC-MZ still achieved a swelling ratio of 50.07% after 24 hours (Figure 4(d)). The CMA single-network hydrogel, featuring a distinctly large-pore structure, exhibited the highest water absorption performance, with a swelling ratio of 68.48%.

Good moisturizing capability allows the dressing to maintain a moist wound environment over an extended period, providing suitable conditions for healing. High water absorbency enables effective uptake of exudate, promoting the healing process. These two properties are complementary and indispensable. However, existing materials often struggle to balance both. For instance, Guo Shoucheng et al.[26]introduced poly(p-dioxanone) (PPDO) into the PVA hydrogel network to prepare a PPDO/PVA composite hydrogel. Although its equilibrium swelling ratio reached 67%–75%, it retained only about 5% of its moisture after 20 hours, indicating weak water retention. Wang et al.[27]constructed a lipoic acid-modified chitosan (LAMC) hydrogel via amidation, which exhibited a swelling ratio of only 30%, limiting its capacity to absorb wound exudate. In contrast, the CaPSC-MZ hydrogel prepared in this study achieved a swelling ratio of 50.07% and a water retention rate of 13.13% after 24 hours, striking a favorable balance between water absorption and retention, demonstrating its potential as a high-quality wound dressing.

3.4 Mechanical Properties of CaPSC-MZ Hydrogel

The mechanical properties of hydrogels are crucial for their protective function as wound dressings. If the strength is too low, the hydrogel is prone to rupture, failing to form an effective mechanical barrier for the wound. Conversely, if the strength is too high, it may cause secondary damage to the wound site during friction or movement. Therefore, an ideal wound dressing should possess good flexibility to conform to skin deformations. Existing studies have attempted to improve wound dressings by enhancing mechanical strength or adhesion. For example, Guan et al.[16]utilized cellulose nanocrystals to reinforce a PVA matrix, and Castrejon-Comas et al.[28]developed a hyaluronic acid-based hydrogel. However, these studies did not further evaluate the foldability of the materials, which is key to achieving good skin conformity and adapting to dynamic joint movements in the human body.

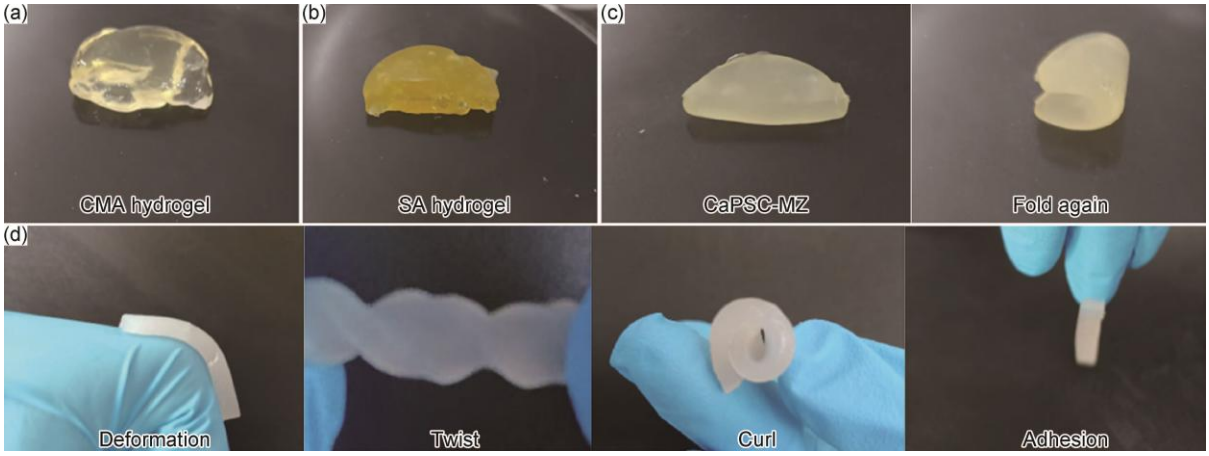

Figure 5 Digital photos of hydrogel samples and their distortion: (a) CMA; (b) SA; (c) CaPSC-MZ; (d) CaPSC-MZ.

Figure 5 characterizes the mechanical properties of CMA, SA, and CaPSC-MZ hydrogels (diameter: 2.5 cm, thickness: 4 mm). As shown in Figures 5(a) and 5(b), upon folding, both CMA and SA hydrogels exhibited evident fractures at the fold lines, with multiple surface cracks visible, indicating poor mechanical properties. In contrast, the CaPSC-MZ hydrogel remained intact at the fold line after folding, with a smooth, undamaged surface (Figure 5(c)). Furthermore, when CaPSC-MZ was subjected to a second fold, the crease remained intact, demonstrating high flexibility in the CaPSC-MZ hydrogel. This property primarily originates from the contribution of the PVA network. To verify its practical conformability, a strip of CaPSC-MZ hydrogel was affixed to a finger joint. The results showed that it not only adhered firmly to the joint surface but also deformed flexibly with joint flexion

and extension, exhibiting good conformability (Figure 5(d)). Additionally, torsion and curling tests on elongated CaPSC-MZ samples revealed no surface cracks, further confirming its excellent mechanical tolerance. Figure 5(d) also presents adhesion tests; the CaPSC-MZ hydrogel could adhere to the finger surface and did not detach under vertical conditions, indicating good adhesive performance.

The aforementioned results indicate that the CaPSC-MZ hydrogel combines a soft texture with excellent mechanical properties, enabling effective adhesion to the skin and reliable mechanical protection for wounds. Its compliant nature prevents secondary damage caused by excessive material stiffness, while its ability to adapt to dynamic skin changes reduces wound irritation from friction, showcasing its potential for application as a wound dressing.

3.5 pH Responsiveness of CaPSC-MZ Hydrogel

During wound healing, the inflammatory and proliferative phases are two temporally sequential yet partially overlapping stages[29–30]. During this period, the pH of the wound microenvironment typically shifts towards the acidic range. To simulate this dynamic change, this study selected pH conditions of 7, 6, and 5[31–32]to investigate the release behavior of Ca2+, Mg2+, and Zn2+from the CaPSC-MZ hydrogel. The results are presented in Figure 6. The cumulative release rates of all three ions increased significantly with decreasing pH. This is primarily attributed to the metal ions being loaded onto the CMA network via binding to deprotonated –COO−groups, thereby stabilizing their presence within the gel system. Under acidic conditions, H+ions compete with metal ions for binding sites, prompting Ca2+, Mg2+, and Zn2+to dissociate from carboxyl groups and diffuse out through the hydrogel matrix. Further comparison of the cumulative release rates at pH = 5 revealed that within 5.15 hours, the cumulative release rates of Mg2+and Zn2+reached 61.99% and 65.23%, respectively, while the release rate of Ca2+was only 24.34%. This discrepancy mainly stems from the differing existence states and binding strengths of Ca2+, Mg2+, and Zn2+within the gel network. Ca2+primarily participates in forming the "egg-box" structure of the SA network, creating stable coordination crosslinks. Consequently, most Ca2+is firmly bound within the network, with only a small fraction of free or weakly bound Ca2+available for release. In contrast, Mg2+and Zn2+exhibit weaker binding affinity with SA and rely mainly on carboxyl groups on CMA chains via weaker ionic bonds, making them more susceptible to displacement by H+under acidic conditions and facilitating rapid release.

In summary, Ca2+, Mg2+, and Zn2+in the CaPSC-MZ hydrogel all exhibit distinct pH-responsive release characteristics, with release rates increasing as the environment becomes more acidic. This release behavior aligns with the dynamic pH changes during the wound healing process, indicating that the CaPSC-MZ hydrogel can release active ions on demand at different healing stages, thereby playing a positive role in modulating the wound microenvironment.

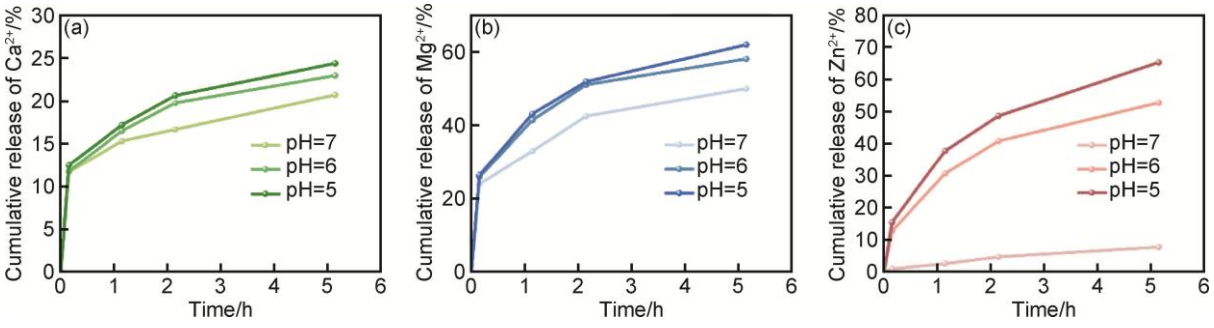

Figure 6 Cumulative release rates of Ca2+(a), Mg2+(b), and Zn2+(c) from CaPSC-MZ hydrogel under different pH conditions.

3.6 Conductivity of CaPSC-MZ Hydrogel

Bioelectrical signals are closely linked to the wound tissue healing process. Applying appropriate external currents can promote cell proliferation and migration, thereby accelerating wound repair. As an ideal wound

dressing material, if a hydrogel possesses good conductivity, it can enable electrical stimulation therapy for wounds.

To investigate the conductive properties of CaPSC-MZ and its single-network components (CMA, PVA), the conductivity of each gel group was tested using an electrochemical workstation (Figure 7). As shown in Figure 7(a), under the condition of a fixed addition of 0.2 mL of CaSO4solution, the conductivity of the CaPSC-MZ hydrogel gradually increased with the volume of the Mg2+/Zn2+mixed solution (0, 0.05, 0.1, 0.15, 0.2, 0.4, 0.6 mL). When the Mg2+/Zn2+addition reached 0.6 mL, the maximum conductivity was 33.72 mS/cm. Notably, the group with simultaneous addition of 0.2 mL CaSO4and 0.2 mL Mg2+/Zn2+mixed solution exhibited a conductivity of 24.81 mS/cm. When only 0.2 mL of CaSO4was added without Mg2+/Zn2+, the system still maintained a conductivity of 14.00 mS/cm due to Ca2+migration, indicating that the introduction of Mg2+/Zn2+significantly enhances the ionic conductivity of the composite hydrogel. Figure 7(b) illustrates the effect of varying volumes of CaSO4solution (0, 0.05, 0.1, 0.15, 0.4, 0.6, 0.8 mL) on conductivity under the condition of a fixed addition of 0.2 mL Mg2+/Zn2+mixed solution. As the CaSO4addition increased, the conductivity gradually improved, reaching a maximum of 22.45 mS/cm at 0.8 mL. It is worth noting that the group with only 0.2 mL Mg2+/Zn2+mixed solution and no Ca2+exhibited a conductivity of merely 11.02 mS/cm, significantly lower than the group with only 0.2 mL CaSO4and no Mg2+/Zn2+. This phenomenon may be attributed to the lack of Ca2+preventing the formation of a stable three-dimensional SA network skeleton, thereby restricting effective ion migration. Although increasing CaSO4aids in elevating conductivity, comparing the data from CaPSC-MZ0.4and Ca0.4PSC-MZ reveals that the former's conductivity (26.18 mS/cm) is higher than the latter's (19.34 mS/cm). This indicates that while Ca2+increases the ionic concentration, its contribution to conductivity is limited by the low solubility of CaSO4. Excessive Ca2+leads to over-crosslinking of SA, increasing the crosslinking density, which in turn hinders ion migration and reduces conductivity. To further explore the impact of crosslinking density on conductive behavior, this study prepared CaP2SC hydrogel with a higher PVA content and lower CMA content.

Figures 7(c) and 7(d) illustrate the trends in conductivity for this hydrogel under varying Mg2+/Zn2+mixed solution volumes (fixed 0.2 mL CaSO4solution; Mg2+/Zn2+volumes: 0, 0.05, 0.1, 0.15, 0.2, 0.4, 0.6 mL) and varying CaSO4addition volumes (fixed 0.2 mL Mg2+/Zn2+mixed solution; CaSO4volumes: 0, 0.05, 0.1, 0.15, 0.4, 0.6, 0.8 mL), respectively. Similar to the CaPSC series, the group without Ca2+but containing Mg2+/Zn2+exhibited a lower conductivity (8.91 mS/cm) than the group with only Ca2+(11.76 mS/cm). Moreover, conductivity increased with the proportion of Mg2+/Zn2+, remaining higher than the corresponding CaSO4addition groups. Additionally, all conductivity values for the CaP2SC series were lower than those of the corresponding CaPSC groups. SEM results indicated that the dense pore structure formed by PVA affects the macroporous morphology of CMA, positioning the pore size of the triple-network hydrogel between the two. Therefore, the higher PVA content in CaP2SC leads to a denser gel structure, which is the primary reason for its lower conductivity. As shown in Figure 7(e), the conductive performance of the hydrogel is jointly regulated by crosslinking density and ion content. Mg2+/Zn2+are the primary contributors to conductivity; however, their function relies on the stable network skeleton constructed by SA. Excessive crosslinking density narrows ion channels and increases migration resistance, thereby lowering conductivity. Synthesizing all results, this study selected Ca0.2PSC-MZ0.2as the standard hydrogel system for subsequent experiments.

Furthermore, Figure 7(f) reveals, through comparison of the conductive properties of single-network and composite networks, that the conductivities of pure PVA and CMA are extremely low, at 7.64 mS/cm and 1.58 mS/cm, respectively. Upon introduction of SA, the conductivity increased to 14.00 mS/cm. Further construction of the CaPSC-MZ triple-network system elevated the conductivity to 24.81 mS/cm.

The aforementioned conductivity test results demonstrate that the CaPSC-MZ hydrogel prepared in this study possesses excellent conductive performance. This is attributed to the conductive network skeleton built by sodium alginate (SA) and Ca2+, synergized with bioactive Mg2+and Zn2+. This hydrogel system achieves high ionic conductivity while maintaining good biocompatibility and mechanical compliance. Compared with similar ion-conductive materials reported in the literature—for instance, Sun et al.[33]prepared a hydrogel based on polyacrylic acid and ionic liquid (IL) with a conductivity of 14.8 mS/cm, and Tao Hui et al.[34]obtained a sodium carboxymethyl cellulose/polyacrylic acid hydrogel with a conductivity of 17.5 mS/cm via Fe3+introduction—the

CaPSC-MZ hydrogel exhibits outstanding conductive performance, showing promising application prospects in the field of wound electrical stimulation therapy.

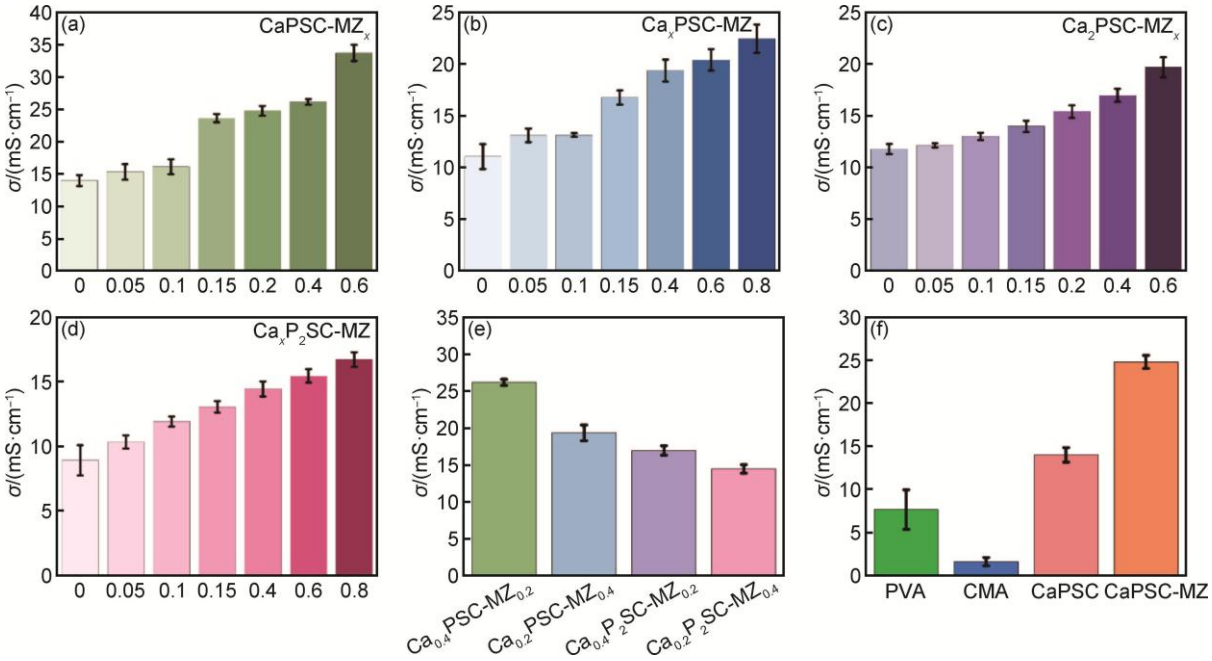

Figure 7 Conductivity of CaPSC-MZ hydrogels (a), CaxPSC-MZ hydrogels (b), CaP2SC-MZ hydrogels (c), CaxP2SC-MZ hydrogels (d), Ca0.4PSC-MZ0.2, Ca0.2PSC-MZ0.4, Ca0.4P2SC-MZ0.2, and Ca0.2P2SC-MZ0.4hydrogels (e), and PVA, CMA, CaPSC, and CaPSC-MZ (f).

3.7 Biocompatibility of CaPSC-MZ Hydrogel

Good biocompatibility is the foundation for the clinical translation of biomedical materials and a core characteristic essential for wound dressings. To evaluate the biocompatibility of the prepared multifunctional hydrogel, different compositions of Ca0.2PSC-MZ0.2hydrogel, Ca0.2PSC-MZ0.4hydrogel, and human skin fibroblasts (HSFs) were co-cultured. Cell morphology observation and activity assays were conducted to comprehensively assess their biological performance. The extracts of Ca0.2PSC-MZ0.2and Ca0.2PSC-MZ0.4hydrogels, along with a PBS control, were co-cultured with HSFs cells, and cell viability was detected on Days 1, 3, and 5. The results in Figure 8 show that compared with the control group (Figure 8(a)), cells in the Ca0.2PSC-MZ0.2group exhibited intact morphology and significant proliferation (Figure 8(b)), indicating no obvious cytotoxicity of this material. Conversely, cell proliferation in the Ca0.2PSC-MZ0.4group was strongly inhibited, with most cells dead (Figure 8(c)), suggesting potent cytotoxicity in this hydrogel group. This toxicity may be associated with excessive Mg2+and Zn2+in the material. High concentrations of Mg2+can interfere with intracellular Ca2+signaling[35], suppressing cell viability. Additionally, excess Zn2+can induce mitochondrial damage and accelerate ATP depletion, ultimately leading to cell death[36–37].

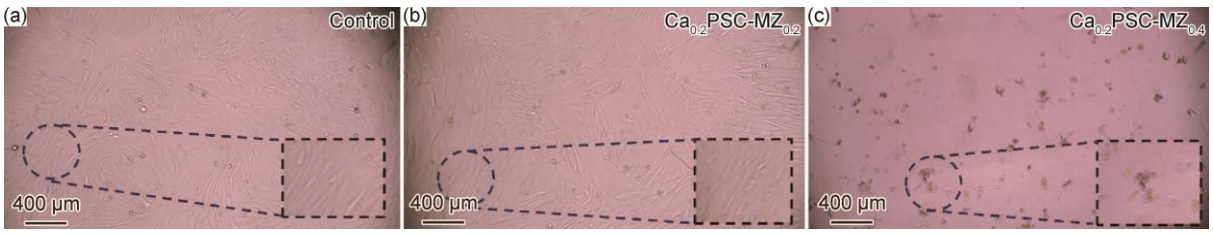

Figure 8 Cell microscopic images of hydrogel: (a) control group; (b) Ca0.2PSC-MZ0.2; (c) Ca0.2PSC-MZ0.4.

CCK-8 quantitative analysis further corroborated the aforementioned results (Figure 9). Compared with the control group, the Ca0.2PSC-MZ0.2group exhibited significantly enhanced cell proliferation, whereas cell activity in the Ca0.2PSC-MZ0.4group fell even below the initial level, confirming its cytotoxicity. The enhanced cell proliferation in the Ca0.2PSC-MZ0.2group can be attributed to the synergistic promotion of cell migration and proliferation by the introduced appropriate amounts of Mg2+and Zn2+. Activation of ERK is crucial for epidermal cell migration, and Mg2+can enhance ERK1/2 phosphorylation, an intracellular signaling factor required for cell migration. Meanwhile, Mg2+activates the MEK/ERK/MMP-7 axis, thereby promoting keratinocyte migration[38]. Zn2+can drive macrophage polarization towards the M2 phenotype via IL-4-induced Jak-STAT signaling and inhibit NF-κB pathway-mediated polarization towards the M1 phenotype. Furthermore, increased intracellular Zn2+concentration effectively promotes STAT3 phosphorylation, upregulating the expression of α-SMA, COL1, and other downstream genes, and inducing HSF differentiation into myofibroblasts, thereby promoting skin wound healing[39–41]. Moreover, Mg2+can upregulate ZIP6 and ZIP10 expression to facilitate more Zn2+entry into HSFs, further strengthening the aforementioned repair processes.

The aforementioned results indicate that Ca0.2PSC-MZ0.2, i.e., the standard CaPSC-MZ hydrogel, not only possesses good biocompatibility and safety but also contains appropriately loaded Mg2+and Zn2+that effectively promote cell proliferation and migration, playing a positive role in the wound healing process. Therefore, this hydrogel represents a highly promising wound dressing material.

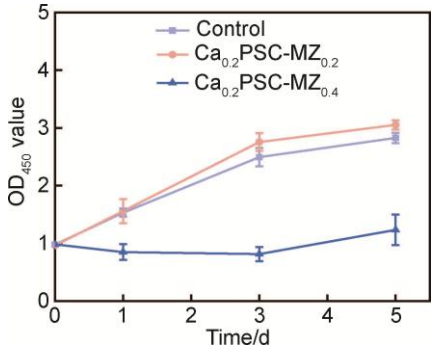

Figure 9 CCK-8 statistics of control group, Ca0.2PSC-MZ0.2, and Ca0.2PSC-MZ0.4hydrogel groups.

The exceptional multifunctionality of the CaPSC-MZ triple-network hydrogel originates from the rational integration of polymeric architecture, ionic crosslinking chemistry, and microenvironmental responsiveness, which collectively overcome the inherent trade-offs in conventional wound dressings. At the structural level, the hydrogel is constructed from three interpenetrating networks with complementary roles: carboxymethyl agarose (CMA) serves as the functional scaffold, where introduced carboxyl groups ($-COO^-$) not only enhance hydrophilicity but also act as dynamic binding sites for bioactive Mg^{2+} and Zn^{2+}. Sodium alginate (SA) forms the ionic conductive backbone via coordination with Ca^{2+}, where guluronic acid-rich G-blocks create electronegative "egg-box" cavities that sequester divalent cations, establishing a stable three-dimensional ionic network. Polyvinyl alcohol (PVA) contributes mechanical robustness through physically crosslinked microcrystalline domains generated by repeated freeze-thaw cycles: during freezing, water crystallization expels PVA chains into amorphous regions, promoting close chain packing and hydrogen bond formation, which reinforces the hydrogel without compromising flexibility. The synergy of these networks yields a hierarchically porous architecture with an average pore size of 91.47 μm—smaller than single-network CMA (209.46 μm) but larger than PVA (44.77 μm)—balancing fluid management: the 50.07% swelling ratio enables efficient uptake of wound exudate, while the densified network from metal ion crosslinking enhances water retention to 13.13%, outperforming many reported PVA-based dressings that sacrifice retention for absorption.

Electrically, the hydrogel achieves high ionic conductivity (24.81 mS/cm) through concerted ion migration: Ca^{2+} within the SA egg-box structure provides baseline conductivity, while Mg^{2+} and Zn^{2+}—weakly bound to CMA carboxyl groups—act as mobile charge carriers. Notably, conductivity is governed by a delicate balance between ionic concentration and crosslinking density: excessive Ca^{2+} induces over-crosslinking of SA, narrowing ion channels and increasing migration resistance, whereas optimal Mg^{2+}/Zn^{2+} loading expands charge carrier availability without disrupting network integrity. Crucially, the hydrogel exhibits pH-responsive ion release

aligned with wound healing dynamics: under acidic inflammatory conditions (pH 5–6), H^+ competitively displaces Mg^{2+} and Zn^{2+} from -COO^- sites, driving accelerated release (61.99% and 65.23% cumulative release within 5.15 h, respectively), while Ca^{2+}—tightly sequestered in SA crosslinks—remains largely retained (only 24.34% release) to maintain structural stability. Biologically, released Mg^{2+} activates the MEK/ERK/MMP-7 axis to promote keratinocyte migration, while Zn^{2+} upregulates STAT3 phosphorylation to induce fibroblast differentiation into myofibroblasts, synergistically accelerating extracellular matrix remodeling. This multi-mechanistic integration—spanning structural mechanics, ion transport, stimuli-responsive release, and cellular signaling—positions CaPSC-MZ as a dynamically adaptive wound care platform.

While the CaPSC-MZ hydrogel demonstrates promising laboratory-scale performance, several critical avenues warrant further exploration to advance its clinical translation and expand its utility in complex wound management. First, in-depth in vivo validation is essential: future studies should evaluate its efficacy in clinically relevant chronic wound models (e.g., diabetic ulcers, pressure sores), with a focus on quantifying how electrical stimulation from the hydrogel's ionic conductivity modulates endogenous bioelectric signals to accelerate healing. Long-term biocompatibility assessments—including systemic ion leaching profiles, immune response profiling, and histopathological analysis of healed tissue—will be pivotal to establishing safety for prolonged wound contact. Second, the current pH-responsive release mechanism could be refined to achieve spatiotemporal precision: integrating enzyme-cleavable linkers or glucose-sensitive moieties could enable dual-responsive release tailored to the evolving wound microenvironment (e.g., triggered release in hyperglycemic diabetic wounds). Third, scalability remains a key bottleneck: optimizing the one-pot synthesis and freeze-thaw process for large-scale production while retaining network homogeneity and ion distribution uniformity will be critical for commercial viability. Process analytical technology (PAT) tools, such as real-time rheological monitoring, could help standardize fabrication parameters to minimize batch-to-batch variability.

Fourth, expanding functionality through modular integration could address unmet clinical needs: incorporating antimicrobial agents (e.g., silver nanoparticles, quaternary ammonium chitosan) or antioxidant moieties (e.g., curcumin-loaded micelles, polyphenol networks) would equip the hydrogel to manage infected or oxidative stress-impaired wounds. Integrating flexible electronics—such as miniature pH sensors or impedance-based wound status monitors—could transform the dressing into a closed-loop smart system, where real-time wound data triggers adjustable electrical stimulation or ion release. Fifth, comparative studies against established clinical dressings (e.g., hydrocolloids, alginate foams) are needed to benchmark performance across key metrics: cost-effectiveness, ease of application/removal, patient comfort, and healing outcomes. Health economic analyses evaluating its impact on reducing dressing change frequency and hospital stay duration would strengthen its value proposition for healthcare systems. Finally, fundamental research into the interplay between ionic conductivity and cellular electrotaxis in vivo could uncover novel mechanistic insights, potentially guiding the design of next-generation bioelectronic dressings that mimic endogenous electrical cues with greater fidelity. By bridging materials science innovation with clinical need-driven engineering, the CaPSC-MZ platform has the potential to evolve from a laboratory prototype into a transformative tool for personalized wound care.

4 Conclusion

(1) This work successfully prepared a conductive triple-network hydrogel, CaPSC-MZ, constructed from CMA, PVA, and SA forming a triple crosslinked network, with Ca2+, Mg2+, and Zn2+loaded within the molecular chains. This material exhibits high water absorbency (50.07%) and high water retention capacity (13.13%), enabling effective absorption of wound exudate while maintaining a moist environment, thereby providing suitable conditions for wound healing.

(2) Through the introduction of PVA, the CaPSC-MZ hydrogel demonstrates excellent flexibility, allowing it to be curled and conformed to dynamic wound morphologies, preventing secondary tissue damage. The CaPSC-MZ hydrogel achieves responsive release of Ca2+, Mg2+, and Zn2+under varying pH conditions, showcasing dynamic responsiveness.

(3) The incorporation of metal ions and the structural characteristics of the SA molecular skeleton endow the hydrogel with excellent ionic conductivity (24.81 mS/cm), laying a solid foundation for its application in electrical

stimulation-accelerated wound healing. Biocompatibility test results confirm that the CaPSC-MZ hydrogel possesses good biosafety and the potential to promote cell proliferation.

References

[1] HUANG W C, YING R, WANG W, et al. A macroporous hydrogel dressing with enhanced antibacterial and anti-inflammatory capabilities for accelerated wound healing[J]. Advanced Functional Materials, 2020, 30 (21): 2000644.

[2] SU R, WANG L L, HAN F, et al. A highly stretchable smart dressing for wound infection monitoring and treatment[J]. Materials Today Bio, 2024, 26: 101107.

[3] SHU H, ZHANG T T, JIANG Y L, et al. Mechanoregulative hydrogel facilitates rapid scarless healing by self-adaptive control of wound niche at different stages[J]. Science Advances, 2025, 11(21): eadv9895.

[4] UBEROI A, MCCREADY-VANGI A, GRICE E A. The wound microbiota: microbial mechanisms of impaired wound healing and infection[J]. Nature Reviews Microbiology, 2024, 22(8): 507-521.

[5] HUANG Y Q, ZHENG J F, ZENG G H, et al. Chitosan-crosslinked polyvinyl alcohol anti-swelling hydrogel designed to prevent abdominal wall adhesion[J]. Materials Today Bio, 2024, 24: 100931.

[6] WANG M, BAI J, SHAO K, et al. Poly(vinyl alcohol) hydrogels: the old and new functional materials[J]. International Journal of Polymer Science, 2021, 16: 2225426.

[7] HUANG Y Q, ZHENG J F, ZENG G H, et al. Chitosan-crosslinked polyvinyl alcohol anti-swelling hydrogel designed to prevent abdominal wall adhesion[J]. Materials Today Bio, 2024, 24: 100931.

[8] SHI C X, WANG H, WANG X J, et al. A safe, stable, simple, serviceable, and self-powered wound dressing with continuous low-voltage direct current electrical stimulation: an efficient approach to accelerate wound healing[J]. Advanced Functional Materials, 2025, 35(29): 2422188.

[9] GHOSH S, KUMAR N, CHATTOPADHYAY S. Electrically conductive “SMART” hydrogels for on-demand drug delivery[J]. Asian Journal of Pharmaceutical Sciences, 2025, 20(1): 101007.

[10] [10] HOU X X, WANG Y J, ZHU M N, et al. GelMA/AgNWs hydrogel combined with electrical stimulation effectively promotes skin wound healing[J]. Advanced Materials Interfaces, 2025, 12(14): e00149.

[11] LI L, XU W Y, XU M Y, et al. Construction of self-healing conductive hydrogel based on polyvinyl alcohol/wool keratin/carbon nanotube[J]. China Plastics Industry, 2024, 52(3): 144-151.

[12] LI H, CAO J, WAN R T, et al. PEDOTs-based conductive hydrogels: design, fabrications, and applications[J]. Advanced Materials, 2025, 37(7): 2415151.

[13] WANG M, ZHENG J J, ZHOU J L. Research progress of PEDOT: PSS-based conductive hydrogels electrodes for ECG monitoring[J]. Journal of Tiangong University, 2025, 44(4): 60-70.

[14] LIN X Y, XU X B, LI X, et al. Liquid metal/cyclodextrin composite biomimetic memory hydrogel[J]. Chinese Journal of Chemical Engineering, 2025, 76(11): 6077-6085.

[15] LEI H, FAN D D. Conductive, adaptive, multifunctional hydrogel combined with electrical stimulation for deep wound repair[J]. Chemical Engineering Journal, 2021, 421: 129578.

[16] GUAN L, OU X L, WANG Z, et al. Electrical stimulation-based conductive hydrogel for immunoregulation, neuroregeneration and rapid angiogenesis in diabetic wound repair[J]. Science China Materials, 2023, 66: 1237-1248.

[17] GONG J P, KATSUYAMA Y, KUROKAWA T, et al. Double-network hydrogels with extremely high mechanical strength[J]. Advanced Materials, 2003, 15(14): 1155-1158.

[18] GHOSAL D, MAJUMDER N, DAS P, et al. Enhancing wound healing with sprayable hydrogel releasing multimetallic ions: inspired by the body's endogenous healing mechanism[J]. Advanced Healthcare Materials, 2024, 13(32): 2402024.

[19] GUO Y N, HUANG W C, MAO X Z. Preparation and release properties of pH responsive carboxymethyl agarose-polydopamine hydrogel[J]. Food Science, 2022, 43(10): 59-65.

[20] ORTIZ J A, SEPULVEDA F A, PANADERO-MEDIANERO C, et al. Cytocompatible drug delivery hydrogels based on carboxymethylagarose/chitosan pH-responsive polyelectrolyte complexes[J]. International Journal of Biological Macromolecules, 2022, 199: 96-107.

[21] KHAN H, CHAUDHARY J P, MEENA R. Anionic carboxymethylagarose-based pH-responsive smart superabsorbent hydrogels for controlled release of anticancer drug[J]. International Journal of Biological Macromolecules, 2019, 124: 1220-1229.

[22] WU J L, HE W Y, XU R J, et al. Asymmetric porous hydrogel encapsulating vulcanized molecular brushes wi th anti-bacterial adhesion, anti-infection, and pro-healing properties towards infected wound treatment [J]. Nanoscale, 2024, 16(44): 20489-20495.
[23] FANG D Y, JIN Y G. Progress in wearable devices for drug delivery[J]. Journal of Materials Engineering, 202 4, 52(8): 76-86.
[24] SCHALY S, ISLAM P, PRAKASH S. Alginate-chitosan hydrogel formulations for VEGFA expressed baculovirus delivery promoting angiogenesis for wound healing and revascularization[J]. European Heart Journal, 202 4, 45(Suppl 1): ehae666.1461.
[25] GONG Y, WANG P, CAO R, et al. Exudate absorbing and antimicrobial hydrogel integrated with multifuncti onal curcumin-loaded magnesium polyphenol network for facilitating burn wound healing[J]. ACS Nano, 2 023, 17(22): 22355-22370.
[26] GUO S C, XING R Q, DU X C, et al. Preparation and properties of poly(p-dioxanone)/polyvinyl alcohol comp osite hydrogels[J]. Polymer Materials Science & Engineering, 2024, 40(1): 57-65.
[27] WANG Y, LIU K, WEI W Y, et al. A multifunctional hydrogel with photothermal antibacterial and antioxidan t activity for smart monitoring and promotion of diabetic wound healing[J]. Advanced Functional Material s, 2024, 34(38): 2402531.
[28] CASTREJON-COMAS V, ALEMAN C, PEREZ-MADRIGAL M M. Multifunctional conductive hyaluronic acid hy drogels for wound care and skin regeneration[J]. Biomaterials Science, 2023, 11(7): 2266-2276.
[29] ALZUBAIDY G, ALHARBI S, ABDULLAH T, et al. Role of electrospun scaffolds at different stages of wound h ealing: advancements, challenges, and future directions[J]. ACS Applied Polymer Materials, 2025, 7(21): 1 3991-14014.
[30] DALISSON B, BARRALET J. Bioinorganics and wound healing[J]. Advanced Healthcare Materials, 2019, 8(1 8): 1900764.
[31] CAO W X, XIA D, ZHOU L X, et al. Antibacterial and antioxidant wound dressings with pH responsive releas e properties accelerate chronic wound healing[J]. Materials Today Physics, 2024, 40: 101316.
[32] ZHOU X H, JIANG H, TIAN J L. Li+/poly(dopamine) composite hydrogel with wound-healing properties[J]. J ournal of Xiangtan University (Natural Science Edition), 2025, 47(4): 103-113.
[33] SUN M N, CHEN W Y, WANG L, et al. Highly conductive ionohydrogenels for humidity sensing[J]. Polymers, 2025, 17(3): 327.
[34] TAO H, ZHANG Y X, CHEN Y Q, et al. Preparation of sodium carboxymethyl cellulose/poly(acrylic acid) con ductive hydrogel and its properties[J]. Journal of Functional Polymers, 2025, 39(1): 34-44.
[35] LI Y Q, WANG J, YUE J J, et al. High magnesium prevents matrix vesicle-mediated mineralization in human bone marrow-derived mesenchymal stem cells via mitochondrial pathway and autophagy[J]. Cell Biology I nternational, 2018, 42(2): 205-215.
[36] MAO C, WANG M, ZHUANG L, et al. Metabolic cell death in cancer: ferroptosis, cuproptosis, disulfidptosis, and beyond[J]. Protein & Cell, 2024, 15(9): 642-660.
[37] PALMER L D, JORDAN A T, MALONEY K N, et al. Zinc intoxication induces ferroptosis in A549 human lung c ells[J]. Metallomics, 2019, 11(5): 982-993.
[38] YOSHINO Y, TERUYA T, MIYAMOTO C, et al. Unraveling the mechanisms involved in the beneficial effects of magnesium treatment on skin wound healing[J]. International Journal of Molecular Sciences, 2024, 25 (9): 4994.
[39] NISHIDA K, HASEGAWA A, YAMASAKI S, et al. Mast cells play role in wound healing through the ZnT2/GPR 39/IL-6 axis[J]. Scientific Reports, 2019, 9: 10842.
[40] YIN L, TANG Q W, KE Q, et al. Sequential anti-infection and proangiogenesis of DMOG@ZIF-8/gelatin-PCL electrospinning dressing for chronic wound healing[J]. ACS Applied Materials & Interfaces, 2023, 15(42): 4 8903-48912.
[41] YANG F, XUE Y J, WANG F L, et al. Sustained release of magnesium and zinc ions synergistically accelerates wound healing[J]. Bioactive Materials, 2023, 26: 88-101.